Fizika Nizkikh Temperatur, 2011, v. 37, No. 4, p. 392–396

Origin of an enhanced colossal magnetoresistance effect in epitaxial $Nd_{0.52}Sr_{0.48}MnO_3$ thin films

V.G. Prokhorov and G.G. Kaminsky

Institute of Metal Physics, NASU, Kiev 03142, Ukraine
E-mail: pvg@imp.kiev.ua

J.M. Kim, T.W. Eom, J.S. Park, and Y.P. Lee

q-Psi and Department of Physics, Hanyang University, Seoul 133-791, Korea

V.L. Svetchnikov

National Center for HREM, TU Delft 2628AL, The Netherlands

G.G. Levtchenko, Yu.M. Nikolaenko, and V.A. Khokhlov

Donetsk Institute for Physics and Technology, NASU, Donetsk 83114, Ukraine

Received June 18, 2010

$Nd_{0.52}Sr_{0.48}MnO_3$ films with the different thickness have been prepared by dc magnetron sputtering on $LaAlO_3$ (001) single-crystalline substrates. A decrease of the film thickness leads to a significant suppression of the ferromagnetic (FM) ordering and the Curie point becomes below the antiferromagnetic (AFM) transition temperature. As this take place, a huge rise of the magnetoresistance ratio from 400 to 60 000% at an applied magnetic field of 5 T is observed. We consider that this new kind of the enhanced colossal magnetoresistance effect is originated from the FM/AFM competition and the collapse of the charge-ordered state at high magnetic field rather than through the regular double-exchange mechanism.

PACS: **71.30.+h** Metal–insulator transitions and other electronic transitions;
75.47.Gk Colossal magnetoresistance;
75.47.Lx Magnetic oxides.

Keywords: colossal magnetoresistance, charge ordering, percolation, magnetic films.

1. Introduction

Hole-doped manganites $L_{1-x}A_xMnO_3$, where L and A are a trivalent lanthanide ion and a divalent alkaline-earth ion, respectively, have attracted considerable attention due to their interesting fundamental science, connected with colossal magnetoresistance (CMR), and potential for applications [1]. The CMR phenomenon is traditionally interpreted by a competition between the double-exchange (DE) which leads to the ferromagnetic (FM) metal state and the cooperative Jahn–Teller effect with resulting in a polaron localization at temperature above the Curie point (T_C). However, it was shown recently that the incorporation of the antiferromagnetic (AFM) interaction can be drastically enhance a CMR effect, increasing the magnetoresistance (MR) ratio as large as 10 000% [2]. In this case the CMR is associated with the development of short-distance correlations among polarons, above T_C, resembling the charge arrangement of the charge-ordered (CO) state, which is stabilized by the AFM interactions. Therefore, the experimental observation of a such enhanced CMR effect is more expected in the manganites with $T_N \gtrsim T_C$, where T_N is the Néel temperature. The $Nd_{0.52}Sr_{0.48}MnO_3$ thin film is a more suitable object for a check on this theoretical approach, because manifests a presence of the FM and AFM phases, the transition temperature of which can be controlled by the deposition mode [3]. Moreover, it was shown that both phases are formed from the paramagnetic state and exist separately to each other.

© V.G. Prokhorov, G.G. Kaminsky, J.M. Kim, T.W. Eom, J.S. Park, Y.P. Lee, V.L. Svetchnikov, G.G. Levtchenko, Yu.M. Nikolaenko, and V.A. Khokhlov, 2011

In this paper we report the experimental results for $Nd_{0.52}Sr_{0.48}MnO_3$ films deposited on $LaAlO_3$ (001) single-crystalline substrate. The origin of an enhanced CMR effect is discussed in detail.

2. Experimental techniques

The films were prepared by dc magnetron sputtering at a substrate temperature of 650 °C [4]. Under these conditions the $Nd_{0.52}Sr_{0.48}MnO_3$ (NSMO) films with a thickness of $d \simeq$ 50, 110 and 160 nm were deposited on $LaAlO_3$ (001) (LAO) single-crystalline substrate. The θ–2θ x-ray diffraction (XRD) patterns were obtained using a Rigaku diffractometer with Cu K_α radiation. The lattice parameters evaluated directly from the XRD data were plotted against $\cos^2\theta/\sin\theta$. From the intercept of the extrapolated straight line to $\cos^2\theta/\sin\theta = 0$, a more precise lattice parameter was obtained. The high-resolution electron-microscopy (HREM) study was carried out using a Philips CM300UT-FEG microscope with a field emission gun operated at 300 kV. The point resolution of the microscope was in the order of 0.12 nm. The cross-sectional specimens were prepared by the standard techniques using mechanical polishing followed by ion-beam milling at a grazing incidence. All microstructure measurements were carried out at room temperature. The resistance measurements were made by the four-probe method in a temperature range of 4.2–300 K and a magnetic field up to 5 T. The field-cooled (FC) and the zero-field-cooled (ZFC) magnetization curves were taken with a Quantum Design SQUID magnetometer for the in-plane magnetic field orientation. The magnetization curves obtained for the bare substrates were extracted from the raw experimental curves.

3. Microstructure

Figure 1,*a* presents the θ–2θ XRD scans for NSMO films with $d \simeq$ 50 and 160 nm. Only the fundamental Bragg peaks of high intensity for the film (F) and the substrate (S) are observed, indicating that the deposition results in a highly *c*-oriented crystal structure. It is confirmed by analysis of the transmission contrast of the HREM images. Figure 1,*b* shows the cross-sectional HREM image for thick NSMO film ($d \simeq$160 nm). Inset A in Fig. 1,*b* is the high-magnification same image taken from the [010] zone axis, including the film/substrate interface. It is seen that the film manifests the atomically clean and sharp interface without an amorphous intermediate layer or precipitations. The epitaxial relationship for film and substrate is determined to be $[001]_{NSMO} || [001]_{LAO}$. It is confirmed by the corresponding fast Fourier transform (FFT) for the HREM image, represented by inset B in Fig. 1,*b*, which reveals the almost rectangular pattern only of basic Bragg spots. According to a microstructure analysis, the prepared films have the orthorhombic crystal structure with lattice parameters $a \simeq b \simeq$ 0.387, 0.383 and 0.379 nm, $c \simeq$ 0.388,

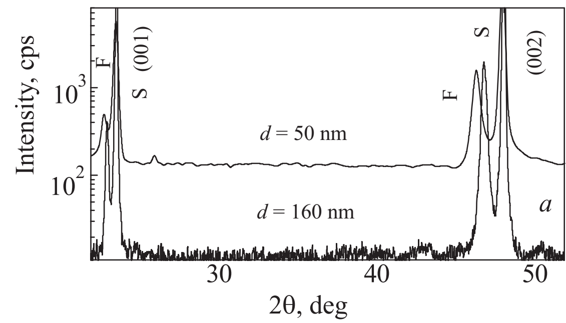

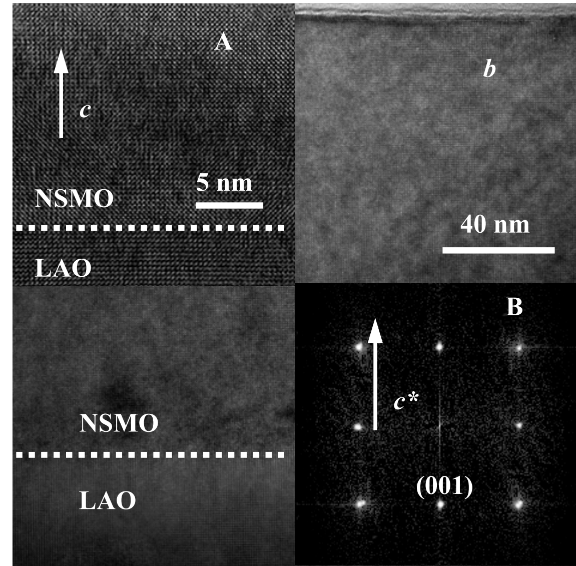

Fig. 1. (*a*) XRD scans for the NSMO films with different thickness. F and S indicate the fundamental Bragg peaks for the film and the substrate, respectively. (*b*) The low-magnification cross-sectional HREM image taken at room temperature for thick film (d = 160 nm). Inset A is the high-magnification cross-sectional HREM image for the same film. Inset B is FFT of the HREM image in A. Dashed lines indicate the film/substrate interface. White arrows indicate the out-of-plane axis.

0.39 and 0.394 nm for $d \simeq$ 160, 110 and 50 nm, respectively, that very close to the published results [5,6].

Therefore, one can conclude that all deposited films have a homogeneous microstructure without the intermediate layer [7] and the column-like texture [8–10]. On the other hand, the lattice mismatch between the film and the substrate (≃2%) leads to a biaxial compressive in-plane and a tensile out-of-plane strains.

4. Experimental results of magnetic and transport properties

Figure 2 shows the in-plane FC temperature dependences of the magnetic moment, $M(T)$, for the NSMO films with thickness $d \simeq$ 50, 110 and 160 nm taken at the magnetic fields of 100 Oe and 1 T. Analysis of low-field FC $M(T)$ curves reveals a significant thickness dependence of the Curie temperature: $T_C \simeq$ 220, 180 and 115 K

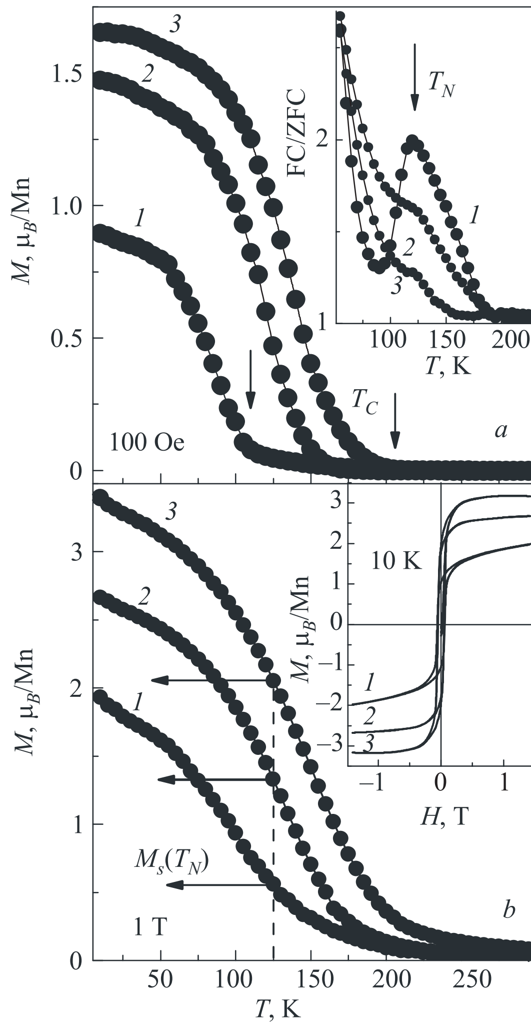

Fig. 2. Temperature dependence of the in-plane FC magnetic moment for the NSMO films with thickness d = 50 (*1*), 110 (*2*) and 160 (*3*) nm at an applied magnetic field of 100 Oe (*a*) and 1 T (*b*). Arrows in *a* indicate the Curie temperature. Inset in *a* is the temperature dependence of the reduced FC/ZFC magnetic moment for the same films at an applied magnetic field of 100 Oe. Arrow marked by T_N indicates the Néel point. Dashed line in *b* indicates the Néel temperature. Horizontal arrows indicate the magnitude of saturated magnetic moment at T_N. Inset in *b* presents the in-plane magnetic hysteresis loops for the same films at 10 K. Lines guide the eye only.

for $d \simeq$ 160, 110 and 50 nm, respectively. The Néel temperature T_N was extracted from the reduced magnetic moment temperature dependence, $M_{FC} / M_{ZFC}(T)$, at H = 100 Oe (represented by the inset in Fig. 2,*a*) and being almost the same for all films, $T_N \simeq 125$ K. The peak position for the thinner film or the well-defined kink for the thicker ones on $M_{FC} / M_{ZFC}(T)$ curve was associated with onset of the AFM transition (indicated by arrow). Therefore, the Curie temperature drastically decreases with decreasing thickness of the NSMO film and becomes smaller of the Néel point for $d \simeq 50$ nm.

A phenomenon of the lattice-strain influence on the Curie temperature for these films has been already considered in detail [10] on the basis of the Millis model [11]. It was shown that obtained change in the crystal lattice parameters with decreasing thickness can lead to the observed suppression of a spin ordering in the investigated films.

Figure 2,*b* presents the FC $M(T)$ curves for the same films, taken at H = 1 T, which can be treated as temperature dependencies of a saturated magnetic moment. It is confirmed by the magnetic hysteresis loops for the same films, represented by the inset in Fig. 2,*b*, which manifests that a saturation of magnetic moment is reached even at an applied magnetic field of 1 T and a low temperature (10 K).

Figure 3 is the temperature-dependent resistance $R(T)$ for the NSMO films with $d \simeq$ 160, 110 and 50 nm without and with an applied magnetic field of 5 T. It is seen that the thicker and thinner films undergo a complete metal–insulator (MI) transition with decreasing temperature: $T_{MI} \simeq$ 175 and 95 K for $d \simeq$ 160 and 50 nm, respectively.

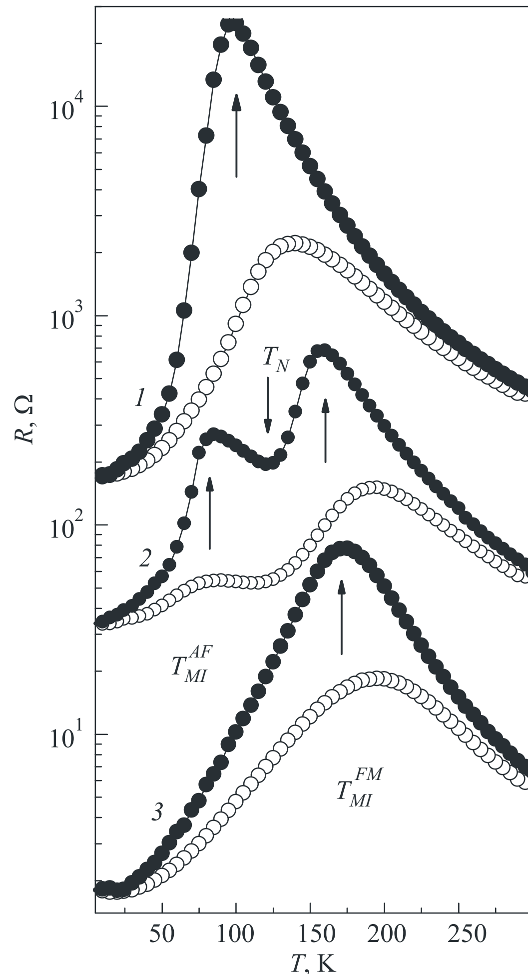

Fig. 3. Temperature dependence of the resistance for NSMO with d = 50 (*1*), 110 (*2*) and 160 (*3*) nm without (solid symbols) and with (open symbols) an applied magnetic field of 5 T. The MI transition temperature is indicated by arrows. T_N indicates the Néel point. Lines guide the eye only.

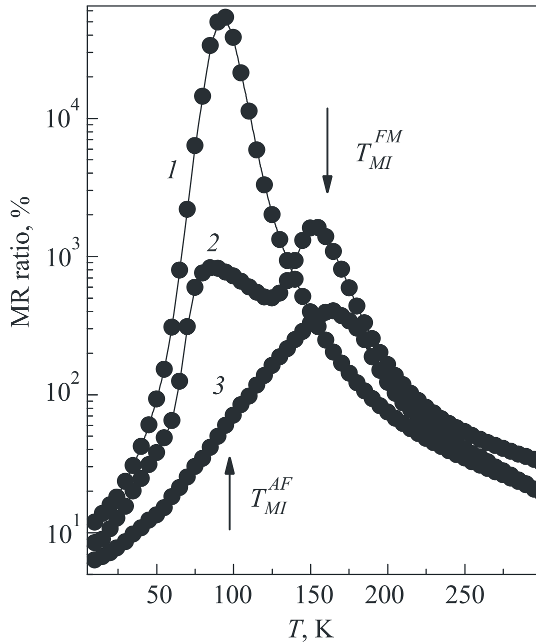

Fig. 4. Temperature dependence of the MR ratio for NSMO with $d = 50$ (*1*), 110 (*2*) and 160 (*3*) nm. Lines guide the eye only.

At the same time, the film with $d \simeq 110$ nm manifests two MI transitions at 160 and 85 K, which are sensitive to an applied magnetic field. This effect can not be explained by the existence of an additional FM phase with different Curie point, because the FM $M(T)$ dependence for this film manifests only a single FM transition (see Fig. 2).

Figure 4 presents the temperature dependence of the magnetoresistance ratio for the same films. The MR value is defined by $100\%\cdot[R(0)-R(H)]/R(H)$, where $R(H)$ and $R(0)$ are the resistances with and without, respectively, an applied magnetic field of 5 T. The main peculiarity of the investigated films is an enormous rise of the CMR effect with decreasing thickness. Thus, MR $\simeq$ 60 000% for thin film ($d \simeq 50$ nm) while does not exceed 400% for thick one ($d \simeq 160$ nm).

5. Discussion

The following intriguing results need in a discussion: (i) an appearance of a second MI transition with the decreasing temperature in the film of intermediate thickness ($d \simeq 110$ nm) and (ii) an enormous rise of the MR ratio in the thinner film ($d \simeq 50$ nm).

The explanation of the observed peculiarities in $R(T)$ must be taken into account the following experimental facts. First, because the FC $M(T)$ behavior for all films (see Fig. 2) is not changed at the Néel temperature, one can conclude that the AFM phase arises from the precursory paramagnetic state rather than from the formed FM one. Therefore, both the FM and AFM phases are co-existent separately to each other in the film at low temperature $(T \le T_C, T_N)$ and can be treated as a percolating net of the metallic (FM) and insulating (AFM) resistors. It is principal difference between the considering samples and the bulk materials [6] or the half-doped films [12]. Second, using the magnetic hysteresis loops and the FC $M(T)$ dependencies taken at $H = 1$ T, represented by Fig. 2,*b*, one can estimate the concentration of the FM (metal) phase in our films at different temperature as $M_s(T)/M_s^{\text{bulk}}$, where $M_s^{\text{bulk}} \simeq 3.5$ μ_B/Mn is the magnetic moment for the bulk NSMO in the fully FM state [13]. At low temperature $M_s(0)/M_s^{\text{bulk}} \simeq$ 0.49, 0.77 and 0.91, while at the Néel point $M_s(T_N)/M_s^{\text{bulk}} \simeq 0.154$, 0.371 and 0.591 for $d \simeq 50$, 110 and 160 nm, respectively. At the same time a percolation threshold for the 3-dimensional magnetic percolating system is $p_c \simeq$ 0.395 [14–16]. Consequently, two kinds of the resistor circuit can be realized in the film depending on the concentration of the FM metal phase: a parallel-resistor circuit for $M_s(T)/M_s^{\text{bulk}} \ge p_c$ and a series-connected resistor for $M_s(T)/M_s^{\text{bulk}} \le p_c$, where the FM and AFM phases play a role of the separated resistors with a different temperature behavior.

Taking into account all that mentioned above, we suggest the following explanation of the unusual behavior of $R(T)$ for the NSMO films. Thick film ($d \simeq 160$ nm) undergoes the classical MI transition at $T_{MI}^{FM} \simeq$ 175 K through the regular DE mechanism, because $M_s(T)/M_s^{\text{bulk}} \ge p_c$ in whole temperature range and the parallel-resistor circuit is realized only. Therefore, the low-resistance FM metal-like phase shunts the high-resistance AFM phase, which is occurred at $T_N \ll T_C$, and the corresponding $R(T)$ rise with the decreasing temperature, belonging to the CO AFM state, does not recognize on the experimental curve. The similar transition is performed in the intermediate film with $d \simeq$ 110 nm at high temperature, $T_{MI}^{FM} \simeq$ 160 K, which is higher of T_N and not very far from the Curie point, $T_C \simeq 180$ K. At the same time, a concentration of the FM phase ($\simeq 0.371$) does not exceed a percolation threshold at the Néel point, providing the series-resistor circuit between the FM and AFM phases. Figure 3 shows that a resistance sharply increases at $T \le T_N$ that is typical for this compound and explained by the electron localization in the CO AFM state [6,12]. However, in our case the expected $R(T)$ increase with the decreasing temperature does not extend up to low temperature and the resistance begin to decrease below a certain temperature, forming the additional peak in $R(T)$ behavior at $T_{MI}^{AF} \simeq$ 85 K. At this temperature the concentration of the FM phase ($\simeq 0.57$) exceeds a percolation threshold and forms the infinite conducting cluster which shunts the CO AFM resistance. In contrast to the considered films, thin NSMO film ($d \simeq 50$ nm) undergoes the AFM transition above the FM one. Therefore, the observed rise in resistance at $T \le T_N$ with the decreasing temperature is occurred due to formation of the CO AFM state. On further cooling the FM phase appears in the film and completely shunts the AFM one at a low temperature, $T \le T_{MI}^{AF} \simeq$ 95 K, yielding the metal-like behavior of $R(T)$.

The observed large difference in the MR-ratio magnitude between thick and thin films is connected with the different mechanism of the MI transition. In the first case the FM metal-like state arises from the paramagnetic (PM) insulating phase through the DE mechanism. An applied magnetic field increases the Curie point and shifts the MI transition to a high-temperature range, causing a CMR effect. In the second one the PM $\rightarrow$ AFM transition is realized in the film and the FM phase acts as a shunt-resistor. In this case the MI transition has a percolation origin and is provided by a competition between the FM metal-like and the AFM insulating phase concentration. Similar mechanism of CMR was proposed recently, taking into account the stabilization of the CO AFM state among the correlated polaron clusters due to the AFM coupling [2]. The huge drop of the resistance in an applied magnetic field, in this case, is governed by a collapse (melting) of the CO state, which forms an enhanced CMR effect [13].

6. Conclusions

We have demonstrated that the magnetic- and electron-phase states are controlled by a thickness in the $Nd_{0.52}Sr_{0.48}MnO_3$ films. The thick film manifests the almost complete FM ordering and the MI transition is realized through the regular DE mechanism. The film with intermediate thickness manifests an additional MI transition with decreasing temperature, which is provided by the competition between the increasing FM phase and the AFM ordering, and has a percolating origin. The thin film demonstrates the MR ratio as large as $\simeq$ 60 000% at an applied magnetic field of 5 T. The observed enhanced CMR effect in thin film is explained by formation of the CO AFM state at temperature above the Curie point and the collapse of the CO state at high magnetic field. Therefore, the deposition technique enables us to manipulate the origin of the CMR effect in thin $Nd_{0.52}Sr_{0.48}MnO_3$ films that is a first step toward the strongly correlated electron devices.

Acknowledgments

This work was supported by the NRF/MEST through the Quantum Photonic Science Research Center, Korea. V. Svetchnikov is grateful to the financial support of Netherlands Institute for Metal Research.

1. For a review, see *Colossal Magnetoresistance, Charge Ordering and Related Properties of Manganese Oxides*, C.N.R. Rao and B. Raveau (eds.), World Scientific, Singapore (1998); *Colossal Magnetoresistance Oxides*, Y. Tokura (ed.), Gordon and Breach, London (1999); E. Dagotto, T. Hotta, and A. Moreo, *Phys. Rep*. **344**, 1 (2001).
2. C. Şen, G. Alvarez, and E. Dagotto, *Phys. Rev. Lett*. **98**, 127202 (2007).
3. V.G. Prokhorov, G.G. Kaminsky, J.M. Kim, T.W. Eom, J.S. Park, Y.P. Lee, V.L. Svetchnikov, G.G. Levtchenko, A.V. Paschenko, Yu.V. Medvedev, Yu.M. Nikolaenko, G.V. Bukin, and V.A. Khokhlov, *Fiz. Nizk. Temp*. **37**, 141 (2011) [*Low Temp. Phys*. **37**, No. 2 (2011)].
4. V.N. Varyukhin, Yu.V. Medvedev, Yu.M. Nikolaenko, A.B. Mukhin, B.V. Belyaev, V.A. Gritskikh, I.V. Zhikharev, S.V. Kara-Murza, N.V. Korchikova, and A.A. Tikhii, *Technical Phys. Lett.* **35**, 937 (2009).
5. R. Kajimoto, H. Yoshizawa, H. Kawano, H. Kuwahara, Y. Tokura, K. Ohoyama, and M. Ohashi, *Phys. Rev*. **B60**, 6506 (1999).
6. Z.Q. Li, H. Liu, Y.H. Cheng, W.B. Mi, A. Yu, H.L. Bai, and E.I. Jiang, *Physica* **B353**, 324 (2004).
7. W. Prellier, A. Biswas, M. Rajeswari, T. Venkatesan, and R. L. Greene, *Appl. Phys. Lett*. **75**, 397 (1999).
8. Y.H. Hyun, S.Y. Park, Y.P. Lee, V.G. Prokhorov, and V.L. Svetchnikov, *Appl. Phys. Lett.* **91**, 262505 (2007).
9. V.G. Prokhorov, G.G. Kaminsky, V.A. Komashko, Y.P. Lee, S.Y. Park, Y.H. Hyun, J.B. Kim, J.S. Park, V.L. Svetchnikov, V.P. Pashchenko, and V.A. Khokhlov, *Fiz. Nizk. Temp*. **33**, 889 (2007) [*Low Temp. Phys*. **33**, 678 (2007)].
10. V.G. Prokhorov, Y.H. Hyun, J.S. Park, J.B. Kim, G.H. Kim, Y.S. Lee, Y.P. Lee, and V.L. Svetchnikov, *J. Appl. Phys.* **104**, 103901 (2008).
11. A.J. Millis, T. Darling, and A. Migliori, *J. Appl. Phys*. **83**, 1588 (1998).
12. Y. Ogimoto, M. Nakamura, N. Takubo, H. Tamaru, M. Izumi, and K. Miyano, *Phys. Rev*. **B71**, 060403 (2005).
13. J. Geck, D. Buns, C. Hess, R. Klingeler, P. Reutler, M. v. Zimmermann, S.-W. Cheong, and B. Büchner, *Phys. Rev.* **B66**, 184407 (2002).
14. Y. Xiong, S.-Q. Shen, and X.C. Xie, *Phys. Rev*. **B63**, 140418 (2001).
15. V.G. Prokhorov, G.G. Kaminsky, V.A. Komashko, Y.P. Lee, and J.S. Park, *Fiz. Nizk. Temp*. **29**, 885 (2003) [*Low Temp. Phys*. **29**, 663 (2003)].
16. V.G. Prokhorov, V.S. Flis, G.G. Kaminsky, Y.P. Lee, J.S. Park, and V.L. Svetchnikov, *Fiz. Nizk. Temp*. **31**, 213 (2005) [*Low Temp. Phys*. **31**, 161 (2005)].